AADE-17-NTCE-101

Effect of Pressure Drawdown on Near Wellbore Stress Change and Growth of Plastic Zone in Depleted Reservoirs

Saeed Rafieepour, Stefan Z. Miska, Evren Ozbayoglu, and Mengjiao Yu, The University of Tulsa; Jianguo Zhang, Reza Majidi, BP America Inc.

Abstract

Drilling and completion design in challenging situations such as deep-water and depleted reservoirs has attained great attention recently. This is because of the changes in in-situ stresses during production period, which, in turn, significantly alters the stress distribution in the near wellbore region and the size of yielded zone. Designing efficient drilling and well completion strategies require accurate prediction of the near wellbore stress state. Currently developed models are divided into two main categories: time-independent and time-dependent. The time-independent models considers either uniform pressure drop or steady-state flow regime. On the other hand, the time-dependent models are based on a transient flow regime in the reservoir (short term). However, these models cannot be used in depleted reservoirs that have been producing for a sufficient period of time so that the effect of the outer boundary has been felt. The aim of this study is to provide closed-form analytical solutions for prediction of plastic zone radius for elastic perfectly-plastic materials after the fluid flow turns into the pseudo-steady-state flow regime. The equilibrium equations are combined with poroelastoplastic constitutive relations to estimate stress state and the size of plastic zone around the wellbore. Our results confirm a significant growth in the size of plastic region, which requires immediate remedial actions to avoid excessive sanding and borehole instabilities. An extensive sensitivity analysis of rock and fluid properties as well as production control parameters are presented.

Introduction

Nowadays, due to high demands for energy sources, petroleum industry moves towards drilling and production in partially depleted reservoirs or deep-water wells as part of comprehensive field development plan. However, due to reservoir depletion induced by hydrocarbon production, the in-situ pore pressure reduces and consequently the far-field in-situ stresses change. As a result, the lower and upper limits of drilling margin change and the safe drilling margin becomes narrower. Although the pore pressure decreases, the lower limit of mud window is determined by the existence of high pressure zones along the wellbore. During drilling in depleted zones, the improper design of drilling fluid weight, not taking into account the stress changes will result in lost circulation of drilling fluid and an increase of Non-Productive Time (NPT) related to wellbore instability events. Wellbore instability problems due to improper drilling fluid design during drilling operation are reported to impose huge annual cost to the oil industry (Rafieepour et al., 2015a, 2015b). On the other hand, during production from partially depleted reservoirs, exclusion of these effects for the optimization of production operation parameters such as surface flow rate and flowing bottomhole pressure may cause excessive sand production especially in unconsolidated sandstone formations. This excessive sand production may lead to perforation plugging, collapse of horizontal wells, and increases production costs by erosion of pipelines and surface facilities (Wang and Sharma, 2016). With above discussion, it is critical to develop a model to incorporate the in-situ stress changes and accurately predict the formation behavior during drilling and production in partially depleted zones. It is noticeable that the induced stress changes during production not only may cause drilling and production-related problems, but also it may lead casing collapse, reservoir compaction and subsidence, and reactivation of pre-existing faults and induced-seismicity (Segall, 1985; Segall, 1989; Morita et al., 1989; Aadnoy, 1991; Santarelli et al., 1998; Hettema, 2000; Holt et al., 2004; Rafieepour et al., 2016).

The currently-used models for stress distribution in near-wellbore region can be divided into two main categories: elasticity-based and elastoplasticity-based models. A subdivision of existing models include those that consider no flow (or uniform pressure in reservoir) and those that include fluid flow. The literature is rich of the models based on theory of elasticity for both no flow (Aadnoy, 1991; Addis, 1997a) and transient flow cases (Paslay and Cheatham, 1962; Seth and Gray for infinite reservoirs (1967a) and finite reservoirs (1967b); Chen and Teufel, 2001). However, some studies describes that the predictions based on these models are conservative (Bradley, 1979a; 1979b). Shahri and Miska (2013) argued that the flow regime in depleted reservoirs is pseudo steady state (PSS) and developed stress solutions based on poroelasticity theory under plane strain assumption. Later on, Rafieepour and Miska (2017) developed several analytical stress solutions for depleted reservoirs based on pseudo-steady state flow regime under different assumptions such as uniaxial

strain; generalized plane stress, and plane strain with displacement boundary conditions.

The former models based on elastoplasticity models are based on no flow (no pore pressure/with pore pressure) and transient flow regime. Risnes et al. (1982) developed several solutions for stress distribution around wellbore in an elasto-plastic Mohr-Coulomb medium under steady state flow regime. A good review of the axisymmetric wellbore/tunnel stress solutions based on M-C and Hoek Brown (H-B) criteria is given by Brown et al. (1983). McLellan and Wang (1994) presented an elastoplastic model for a strain weakening formation with Mohr-Coulomb yield function considering steady state fluid diffusion during drilling including the filter cake effects and capillary forces. Wang and Dusseault (1994) developed stress distribution around circular openings in elastoplastic medium subjected to repeated hydraulic loading considering steady state flow regime. Bradford and Cook (1994) presented a semi-analytic elastoplastic model for wellbore stability analysis for a Mohr-Coulomb hardening material based on deformation theory. They included a transient solution of diffusivity equation for an infinite reservoir with constant flowing bottomehole and constant far-field in-situ pore pressure. There are several other models based on either brittle deformation or hardening/softening plasticity relations (Papanastasiou and Durban, 1997; Chen and Abousleiman, 2012). None of these models are applicable in partially depleted reservoirs.

Moreover, Poisson's ratio and internal friction angle are the controlling parameters for in-situ stress change and re-distribution of stresses around the wellbore. Recently Baldino et al. (2017) and Rafieepour and Miska (2017) have developed several analytical solutions for Poisson's ratio and friction angle determination from interference well tests, respectively.

As discussed earlier, prediction of the effect of pressure drawdown on the stress distribution and the size of plastic region around the wellbore is critical for design of sanding control strategies as well as borehole integrity assurance in partially depleted reservoirs. Since the flow regime is dominantly pseudo steady state in depleted reservoirs, the transient flow regimes cannot be utilized. In this study, a model is proposed to predict the stress state around the wellbore based on the theory of brittle elastoplasticity. In addition, the effect of various parameters on the radius of plastic zone is investigated.

Constitutive assumptions

A typical behavior of rock under tri-axial loading conditions is given in **Fig. 1a**. Under low stresses, the material behaves elastically until it yields at a so-called yield strength (point A). Beyond the yield strength, a hardening behavior is usually observed and an ultimate (or peak) strength occurs at point B. Subsequently, the material softens and the straining occurs along with strength deterioration. At point C, the material reaches its residual strength. This material behavior can be simplified as shown in Fig. 1b. The material is linearly elastic until the ultimate strength is reached. The hardening plasticity before ultimate strength is assumed negligible for the sake of simplicity. Then, its strength weaken instantaneously and thereafter the behavior is described as perfectly-plastic flow as the loading continues. The pre-failure behavior is simulated based on Biot's theory of poroelasticty. The post-failure stress and strain relations are described by the associated Mohr-Coulomb failure function. Since the material undergoes strain weakening after ultimate strength is reached, the sudden weakening is described by the residual values of the friction angle and cohesion resulting from strength degradation. However, the failure initiation is estimated considering pre-failure values of friction angle and cohesion. In addition to material behavior assumption, several further assumptions have been made for the proposed model. The reservoir is assumed to be homogenous and isotropic. The axi-symmetric condition is assumed. The reservoir thickness is assumed to be constant during the production period, which implies a plane strain condition. Moreover, in the following derivations, the compressive stress and strain are considered positive.

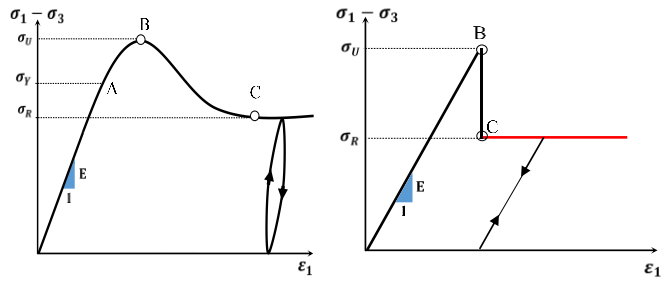

(a) (b)

Fig. 1: Material behavior a) typical experimental observation during triaxial loading b) idealized behavior

Our analysis is in 2-D plane strain and therefore the shearing surfaces are perpendicular to the wellbore plane and limiting the failure modes for the cases where the maximum and minimum principal stresses are in the wellbore plane. Therefore, we limit our analysis for this most common case although there are other permutations of the stress components (Risnes et al., 1982). During drilling and subsequently during production, the wellbore pressure monotonically decreases. This means that the loading continues as the reservoir becomes increasingly depleted without any unloading (fluid injection). Since the wellbore pressure decreases, the radial stress decreases correspondingly while the tangential stress increases ($\acute{\sigma}_{\theta\theta} > \acute{\sigma}_{rr}$). The linear Mohr-Coulomb (M-C) criterion in terms of the radial and tangential stresses, and considering the effect of pore pressure, is described as:

$$\acute{\sigma}_{\theta\theta} - m\acute{\sigma}_{rr} - S_0 = 0 \quad (1)$$

where

$$S_0 = \frac{2c\cos\varphi}{1-\sin\varphi} \quad (2)$$

$$m = \frac{1+\sin\varphi}{1-\sin\varphi} \quad (3)$$

where the effective stresses in equation (1) are described by the Biot's effective stress principle $\acute{\sigma}_{ij} = \sigma_{ij} - \alpha p\delta_{ij}$. However, experimental studies shows that close to the failure, the Biot-Willis coefficient approaches unity (Jaegar et al. 2007).

Model geometry and formulation

Consider a reservoir having a circular drainage area. Initially, the reservoir and surrounding formations are in equilibrium. A vertical wellbore of radius r_w is drilled instantaneously and the local equilibrium is disturbed though replacing the rock materials by a mud with pressure P_w. **Fig. 1** describes the geometry of wellbore and reservoir. After well completion operation, the reservoir is subjected to a constant production flow rate at the inner boundary. As a result of production, the stress state in the reservoir changes due to the coupling nature of fluid flow and deformation in the reservoir. For a short period of time from the beginning of production, the flow regime is transient and therefore the far-field stresses are not affected by the production from the wellbore. However, when the pressure disturbance reaches at the outer radius of the reservoir, the flow regime becomes semi-steady state and the far-field stresses change with pore pressure reduction assuming the rock behavior at the outer boundary remains in elastic region. It is assumed that the formation is initially elastic around the wellbore (the wellbore pressure is higher than the critical wellbore pressure) and there is an over-balanced conditions during drilling. The failure onset occurs first at wellbore wall then develops as a circular plastic zone around the wellbore. The purpose of this study is to determine the production-induced near-wellbore stress changes in the reservoir as a function of time and location.

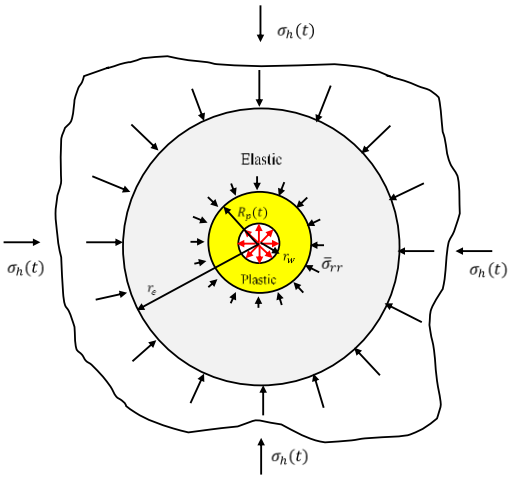

Fig. 2: Model geometry

Pore pressure solution

Assuming weak coupling between the stress and pore pressure (one-way coupling), the fluid flow through porous media is governed by the linear diffusivity equation

$$\frac{\partial^2 p}{\partial r^2} + \frac{1}{r}\frac{\partial p}{\partial r} = C\frac{\partial p}{\partial t} \tag{4}$$

where $C = \frac{\mu C_t \phi}{k}$ is the fluid diffusivity coefficient. Since the flow regime during production from a depleted reservoir is dominantly pseudo-steady state (PSS), therefore the PSS solution has been used in further derivations. The PSS solution for single-phase diffusivity equation is as the following for a cylindrical reservoir

$$p(r,t) = p_i - \frac{5.615\,Qt}{\pi r_e^2 \varphi h c_t} - \frac{141.2\,\mu Q}{kh}\left[ln\left(\frac{r_e}{r}\right) - \frac{3}{4} + \frac{1}{2}\left(\frac{r}{r_e}\right)^2\right] \tag{5}$$

where, c_t is the total compressibility (fluid and pore space) in psi^{-1}, p_i is the initial reservoir pressure in psi, t is time in days, Q is production/injection flow rate in bbl/day, μ is fluid viscosity in cp, r_e is outer radius of the formation in ft, h is reservoir thickness in ft. In this study, the permeability of damaged and undamaged regions are assumed equal.

According to Dake (1998), the time at which the flow regime in a reservoir with circular drainage area turns to the PSS regime can be obtained as

$$t = \frac{948\,\mu C_t \phi r_e^2}{k} \tag{6}$$

where in the above equation t is in hours, μ in cp, C_t in psi^{-1}, r_e in ft and k in md.

Stress solution in elastic region ($r > R_p$)

Based on Biot's three-dimensional theory of consolidation (Biot, 1941), the following relations are given for the stress-strain relationships under drained conditions assuming positive in compression (Wang, 2000)

$$\sigma_{ij} = 2G\varepsilon_{ij} + 2G\frac{\nu}{1-2\nu}\varepsilon_{kk} + \alpha p\delta_{ij} \tag{7}$$

The strain-displacement equations are as the follows for axi-symmetric plane strain deformation conditions:

$$\varepsilon_{rr} = \frac{du}{dr} \qquad \varepsilon_{\theta\theta} = \frac{u}{r} \qquad \varepsilon_{zz} = 0 \tag{8}$$

where all other components of strain tensor are zero and u denotes radial displacement. The equilibrium equation for the plane strain conditions reduces to

$$\frac{d\sigma_r}{dr} + \frac{\sigma_r - \sigma_\theta}{r} + F_r = 0 \tag{9}$$

Combining the strain-displacement equations (8) and stress-strain relations (7), and then substituting into the equilibrium equation, we obtain

$$\frac{\partial^2 u}{\partial r^2} + \frac{1}{r}\frac{\partial u}{\partial r} - \frac{u}{r} + \frac{\eta}{G}\frac{\partial p}{\partial r} = 0 \tag{10}$$

and $\eta = \frac{\alpha(1-2\nu)}{2(1-\nu)}$.The solution for the displacement equation is as:

$$u = \frac{c_1 r}{2} - \frac{\eta}{G}\frac{1}{r}\int_{R_p}^{r} \tilde{r}p(\tilde{r},t)d\tilde{r} + \frac{c_2}{r} \tag{11}$$

The solution (11) together with equations (8) and (7) gives

$$\sigma_{rr} = \frac{G}{1-2\nu}C_1 + \frac{2\eta}{r^2}\int_{R_p}^{r} \tilde{r}p(\tilde{r},t)d\tilde{r} - \frac{2G}{r^2}C_2 \tag{12}$$

$$\sigma_{\theta\theta} = \frac{G}{1-2\nu}C_1 - \frac{2\eta}{r^2}\left[\int_{R_p}^{r} \tilde{r}p(\tilde{r},t)d\tilde{r} - r^2 p(r,t)\right] + \frac{2G}{r^2}C_2 \tag{13}$$

σ_{zz} can be defined as the following relation based on the fact that we have assumed a long reservoir in which the axial strain is zero (both elastic and plastic). With this assumption, we have

$$\sigma_{zz} = \nu(\sigma_{rr} + \sigma_{\theta\theta}) + (1-2\nu)\alpha p \tag{14}$$

The constants of integration in (12) and (13) can be determined using the pore pressure solution given by equation (5) along with the following boundary conditions

$$\sigma_{rr}\left(r=R_p\right)=\bar{\sigma}_{rr} \quad \sigma_{\theta\theta}\left(r=R_p\right)=\bar{\sigma}_{\theta\theta} \tag{15}$$

$$\sigma_{rr}(r=r_e,t)=\sigma_{\theta\theta}(r=r_e,t)=\sigma_h(t) = \frac{v}{1-v}\sigma_{zz}+2\eta p(r_e,t) \tag{16}$$

where $\bar{\sigma}_{rr}$ and $\bar{\sigma}_{\theta\theta}$ are the radial and tangential stresses at the elastic and plastic boundary. It should be noted that the stresses at the outer boundary of reservoir are not constant as described by the equation (16).

After replacing the PSS solution into equations (12) and (13) and integration, we have the following equations for radial and tangential stresses, respectively (Rafieepour and Miska, 2017):

$$\sigma_{rr}(r,t)=\sigma_{rr}(r_e,t)\left[1-\left(\frac{R_p}{r}\right)^2\right]+\sigma_{rr}\left(R_p,t\right)\left(\frac{R_p}{r}\right)^2+\frac{141.2\mu Q}{kh}\eta\left[ln\left(\frac{r}{r_e}\right)+\left(\frac{R_p}{r}\right)^2 ln\left(\frac{r_e}{R_p}\right)+\frac{1}{4}\left(1-\left(\frac{R_p}{r}\right)^2\right) -\frac{1}{4}\frac{1}{{r_e}^2-{R_p}^2}\frac{r^4-{R_p}^4}{r^2}\right] \tag{17}$$

$$\sigma_{\theta\theta}(r,t)=\sigma_{rr}(r_e,t)\left[1+\left(\frac{R_p}{r}\right)^2\right]-\sigma_{rr}\left(R_p,t\right)\left(\frac{R_p}{r}\right)^2-\frac{141.2\mu Q}{kh}\eta\left\{\left[ln\left(\frac{r}{r_e}\right)+\left(\frac{R_p}{r}\right)^2 ln\left(\frac{r_e}{R_p}\right)+\frac{1}{4}\left(1-\left(\frac{R_p}{r}\right)^2\right) -\frac{1}{4}\frac{1}{{r_e}^2-{R_p}^2}\frac{r^4-{R_p}^4}{r^2}\right] +\left[-2ln\left(\frac{r}{r_e}\right)-\frac{3}{2}+\left(\frac{r}{r_e}\right)^2\right]\right\} \tag{18}$$

The overburden stress is obtained from equation (14). It is understood that the material in elastic side of this boundary is on the verge of yielding. Therefore the stresses must satisfy the yield function

$$\left(\bar{\sigma}_{\theta\theta}-\alpha p\left(R_p,t\right)\right)-m\left(\bar{\sigma}_{rr}-\alpha p\left(R_p,t\right)\right)=S_0 \tag{19}$$

Moreover, from equations (17) and (18), it is clear that:

$$\bar{\sigma}_{rr}+\bar{\sigma}_{\theta\theta}=2\sigma_{rr}(r_e,t)+2\eta\left(p\left(R_p,t\right)-p_i+\frac{5.615\ Qt}{\pi r_e^2\varphi hc_t}\right) \tag{20}$$

Combining equation (19) and (20) results in the following equations for stresses on the elastic side of the elastic/plastic boundary (R_p^+)

$$\bar{\sigma}_{rr}=\frac{2\sigma_{rr}(r_e,t)-S_0}{m+1}+\frac{(\alpha(m-1)+2\eta)}{m+1}p\left(R_p,t\right)-\frac{2\eta}{m+1}p_i+\frac{2\eta}{m+1}\frac{5.615\ Qt}{\pi r_e^2\varphi hc_t} \tag{21}$$

$$\bar{\sigma}_{\theta\theta}=\frac{2m\sigma_{rr}(r_e,t)+S_0}{m+1}+\frac{(2\eta-\alpha)m+\alpha}{m+1}p\left(R_p,t\right)-\frac{2\eta m}{m+1}p_i+2\eta\frac{m}{m+1}\frac{5.615\ Qt}{\pi r_e^2\varphi hc_t} \tag{22}$$

The radius corresponding to elastic/plastic boundary is required to obtain the stresses at the elastic/plastic boundary, which will be discussed later. It is possible to obtain the critical wellbore pressure under which a shear failure occurs firstly at the wellbore wall. This is obtained simply by solving the following boundary condition at the wellbore surface

$$\bar{\sigma}_{rr}=(p_w)_{critical} \tag{23}$$

Noting that $p\left(R_p,t\right)=p_w$, we obtain:

$$(p_w)_{critical}=\frac{1}{2-2\eta}(2\sigma_{rr}(r_e,t)-S_0-2\eta p_i) \tag{24}$$

Stress solution in plastic region ($r_w \le r \le R_p$)

Combining the equilibrium equation and active yield function and ignoring the body forces and after integration, the following equation for the radial stress in in plastic region is obtained

$$\sigma_{rr}^p(r,t)=\frac{\alpha(1-m)}{r^{1-m}}\int_{r_w}^{r}\frac{p(\tilde{r},t)}{\tilde{r}^m}d\tilde{r}+\frac{S_0}{1-m}\left[1-\left(\frac{r_w}{r}\right)^{1-m}\right]+p_w(t)\left(\frac{r_w}{r}\right)^{1-m} \tag{25}$$

where $p_w(t)$ is the pressure in wellbore location. It is assumed that the pore pressure and wellbore pressure are equal in reservoir horizon (no mud cake). In the next step, we substitute the PSS flow solution into the above equation and after integration and several further steps, the following solution can be obtained for the radial stress in plastic region

$$\sigma_{rr}^p(r,t)=p_w(t)\left(\frac{r_w}{r}\right)^{1-m}+\left(\frac{S_0}{1-m}+\alpha p_i-\alpha\frac{5.615\ Qt}{\pi r_e^2 hc_t\varphi}\right)\left[1-\left(\frac{r_w}{r}\right)^{1-m}\right]+\alpha\frac{141.2\ \mu Q}{kh}\left[ln\left(\frac{r}{r_e}\right)+\left(\frac{r_w}{r}\right)^{1-m}ln\left(\frac{r_e}{r_w}\right) -\frac{(3m+1)}{4(1-m)}\left[1-\left(\frac{r_w}{r}\right)^{1-m}\right] -\frac{r^2}{2r_e^2}\frac{1-m}{3-m}\left[1-\left(\frac{r_w}{r}\right)^{3-m}\right]\right] \tag{26}$$

The tangential stress in the plastic region can be obtained from equation (1) as

$$\sigma_{\theta\theta}^p\left(R_p,t\right)=m\sigma_{rr}^p(r,t)+(m-1)\alpha\left[p_i-\frac{5.615\ Qt}{\pi r_e^2\varphi hc_t} -\frac{141.2\ \mu Q}{kh}\left[ln\left(\frac{r_e}{r}\right)-\frac{3}{4} +\frac{1}{2}\left(\frac{r}{r_e}\right)^2\right]\right]+S_0 \tag{27}$$

In addition, at the elastic/plastic boundary, the radial stress is obtained by replacing R_p in the above equation. Material is at its initial yield at the elastic/plastic boundary. At the boundary of elastic and plastic regions, the radial stress is continuous, namely

$$\bar{\sigma}_{rr}=\sigma_{rr}^p\left(r=R_p\right) \tag{28}$$

This provide an implicit relation for the radius of plastic region which is function of time and rock and fluid properties should be solved numerically using standard methods such as Newton-Raphson.

Results and discussion

In this section, the results of the analytical models proposed in previous sections for pore pressure and stress distribution in reservoir are presented. The data for the simulations are given in **Table 1**.

Table 1: Data used for stress distribution around the wellbore in depleted reservoirs

Parameter	Value	Symbol
Initial Horizontal Stress, psi	11000	σ_{zz}^{0}
Initial pore pressure, psi	7000	p_0
Porosity, %	20	ϕ
Fluid compressibility, $\mathbf{10^{-6}}$ psi	2.86	C_f
Drained bulk compressibility, $\mathbf{10^{-6}}$ psi	0.862	C_b
Unjacketed compressibility, $\mathbf{10^{-6}}$ psi	0.181	C_S
Drained Poisson's ratio	0.15-0.33	ν
Friction angle, degrees	10-45	φ
Cohesion, MPa	0-10	C
Viscosity, cp	5	μ
Permeability, md	10	k
Flow rate, bbl/day	200	Q
Wellbore radius, ft	0.328	r_w
Outer radius, ft	5000	r_e
Reservoir's thickness, ft	30	h

Fig. 3 shows the pressure profile as a function of time and location. According to the data shown in Table 1 and using the equation (6), the flow regime becomes PSS after 124 days from the begining of production. In PSS flow regime, the time rate of change of pressure is constant.

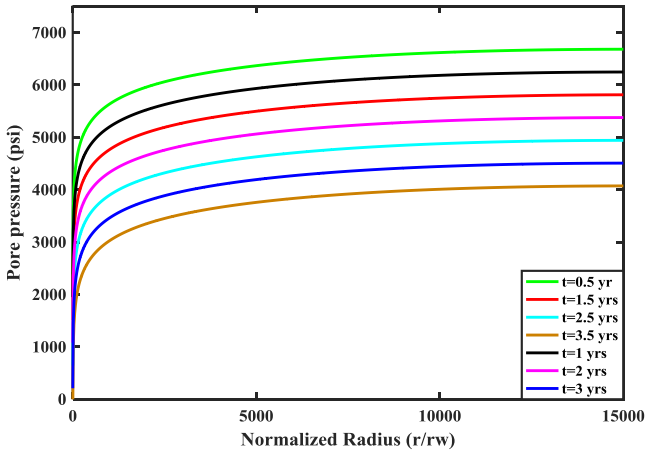

Fig. 3: Pressure profile with time

Stresses in elastic region

Fig. 4 shows flow-induced (hydraulic) component of the radial and tangential stresses. From equations (17) and (18), the hydraulic component of stresses is stationary. In other words, as **Fig. 4** states, these components are time-independent. The radial stress is tensile in the whole domain and is nil in both boundaries and shows a minimum close to the wellbore. On the other hand, the tangential stress is monotonically increasing and it is negative first and becomes positive (compressive) farther from the wellbore wall. The Poisson ratio assumed to be 0.15.

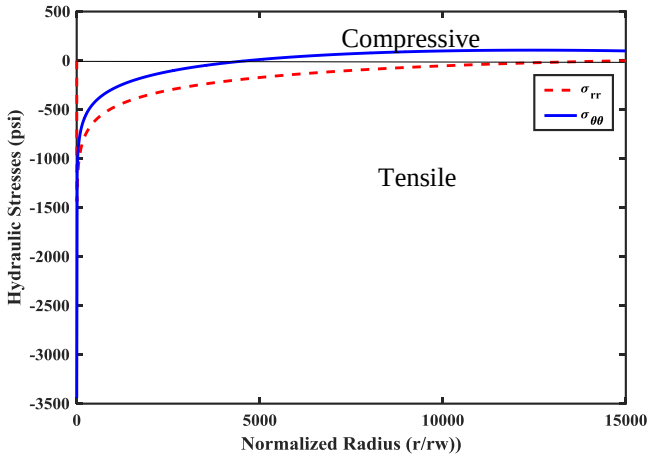

Fig. 4: Flow-induced radial and tangential stresses

Stresses in plastic region

The poroelastic and poroelastoplastic solutions of radial and tangential stresses after two years of production are depicted in **Fig. 5** for the data given in **Table 1** and for a friction angle and cohesion of 20 degrees and 300 psi, respectively. According to this figure, the elastic tangential and radial stresses decrease, respectively, around the wellbore and they reach to the undisturbed in-situ stress field at the dimensionless radii greater than 10. On the other hand, in plastic zone (dimensionless radius of plastic zone is 42), the radial stress increases monotonically and is always lower than the poroelastic radial stress. The tangential stress, however, increases rapidly in the radii close to wellbore upto a maximum value and therafter it decreases slowly at higher distances away from the wellbore. The radial and tangential stresses approach to their poroelastic couterparts at dimensionless radii greater than 120. Moreover, the stresses are releived in plastic region.

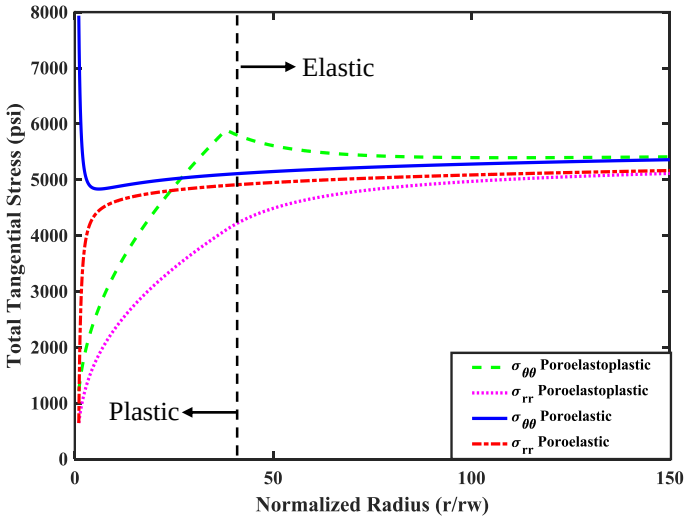

Fig. 5: Radial and tangential stresses around the wellbore: poroelastic and poroelastoplastic (t=2 years)

Fig. 6a and b shows total radial and tangential stresses in the reservoir at different times, namely 0.5, 1, 1.5, 2, 2.5, 3, and 3.5 years after the start production. Again a friction angle and

cohesion of 20 degrees and 300 psi, respectively is assumed. According to **Fig. 7a**, total radial stress in both regions decreases as time progresses. Moreover, the radius of plastic region evolves with time. More clearly, the peak of the total tangential stress depicted in **Fig. 6b** progresses towards the inside of formation with time and, for instance, the dimensionless radius of plastic region increases from 32.6 to 42 after 183 days and 3.5 years from the start of production.

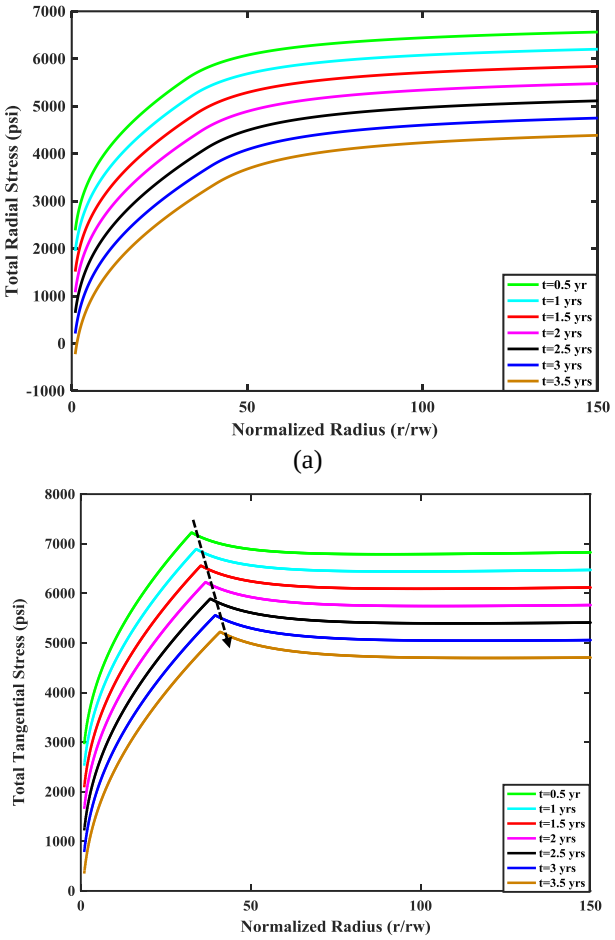

Fig. 6: Radial and tangential stress around the wellbore with time

Fig. 7a and b indicate total axial stress as a function of time and space using poroelastic and poroelastoplastic brittle models, respectively. A comparison of the poroelastic and poroelastoplastic axial stresses around the wellbore (in the similar radius as the size of plastic region in **Fig. 7b**) reveals a similar behavior as we discussed in **Fig. 6** for radial and tangential stresses. With the occurrence of the shear failure, the axial stress relieves and, for example, it reduces to 4000 psi after 3.5 years of production at a dimensionless radius of 2 around the wellbore as compared to a value of 5000 psi estimated by the elasticity solution (1000 psi difference).

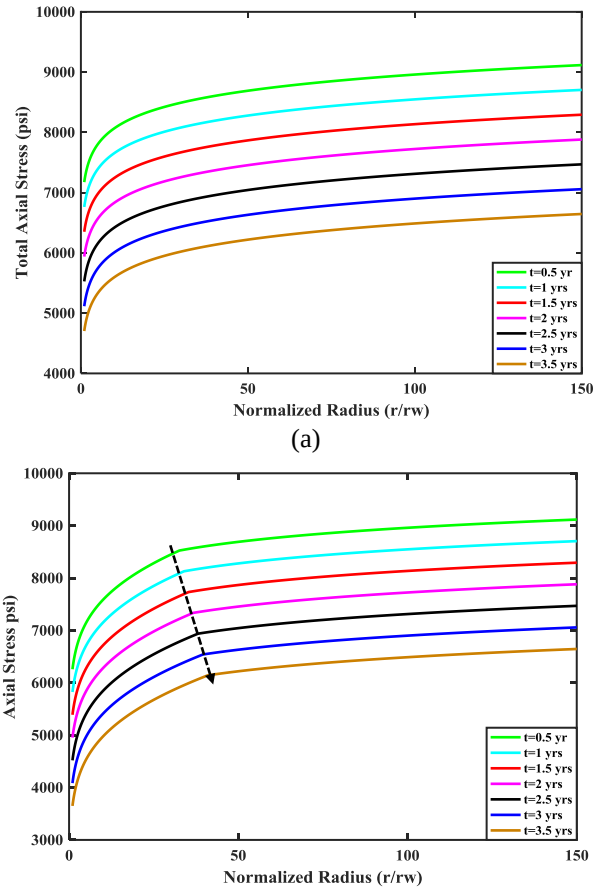

Fig. 7: Axial stress around the wellbore with time

Sensitivity analysis on the effect of various factors on the radius of plastic zone

A review of the relation describing the size of the plastic region reveals that the parametres controling the radius of plastic zone can be categorized as initial in-situ stress and pore pressure; rock properties such as internal friction angle, cohesion, Poisson's ratio, porosity, permeability, total compressibility, and Biot-Willis coefficient; fluid properties such as viscosity; and operational parameters such as flow rate.

Strength and mechanical properties of formation

Fig. 8 is a plot of normalized plastic radius development under different friction angles during production for a 220 psi cohesion. The plastic zone propagates as the wellbore pressure reduces with time (here we plotted the size of plastic zone as a function of time). Moreover, the plot indicates how significant the friction angle can affect the radius of plastic region. For values of friction angles as low as 10°, the size of the plastic zone increases from 1000 normalized radius in the first 183 days to 2100 after 3.5 years of production. The vertical axis scale has been changed to a log scale in order to observe the changes in the radius of plastic zone for higher values of friction angle. From this figure, the radius of plastic zone may be completely disappeared for high values of friction angles.

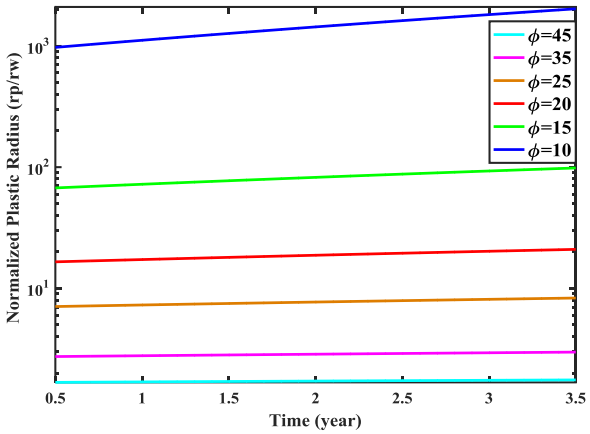

Fig. 8: Effect of friction angle on radius of plastic zone

Fig. 9 shows the plot of normalized plastic radius as a function of time and the cohesive strength for 20° friction angle. The size of plastic zone progressively increases as the cohesive strength decreases. Moreover, this plot indicates that the growth of plastic zone would be higher at lower cohesive strength. However, a comparison of the effect of cohesive strength and friction angle confirms that the friction angle has higher influence on the size of the plastic region. In other words, when the weakening of material is dominated by the loss of friction angle, much plastic zone growth will occur.

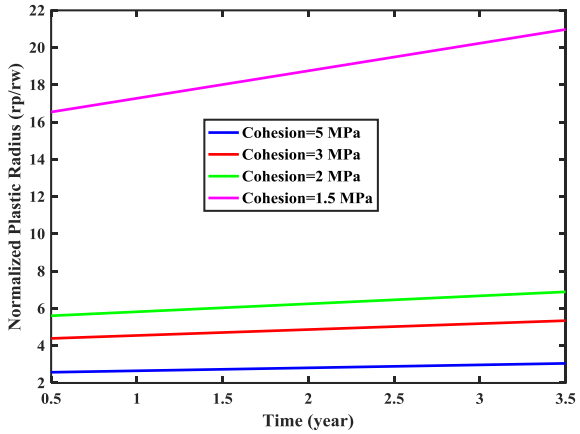

Fig. 9: Effect of cohesion on radius of plastic zone

Fig. 10 describes the effect of Poisson's ratio on radius of plastic zone for cohesive strength and friction angle of 220 psi and 15°, respectively. The size of plastic zone is larger for higher values of Poisson's ratio. Higher values of Poisson ratio indicates that the rock material is less compressible as well as it is a measure of stress transfer to the transverse direction. During drilling and subsequently during production, the radial stress is lower than the tangential stress. This means that for higher values of Poisson's ratio, larger tensile stresses is transferred in the radial direction. Moreover, the rate of plastic radius growth increases with Poisson's ratio.

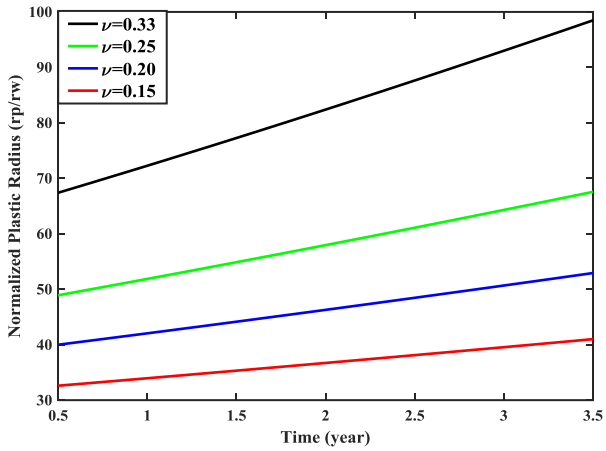

Fig. 10: Effect of Poisson's ratio on radius of plastic zone

Fig. 11 is a plot of normalized plastic radius development under different total rock compressibility during production for a 440 psi cohesion and 15° friction angle. In reservoir engineering texts, total compressibility is defined as: $C_t = C_f + C_r$. The definition of rock compressibility (C_r) in this equation is for non-deformable porous medium with constant bulk volume as given by the following equation (Chen et al., 1995):

$$C_r = \frac{1}{\phi}\frac{\partial \phi}{\partial p}\bigg|_{\varepsilon_{kk}=0} = [(\alpha - \phi)/\phi]C_s \qquad (29)$$

The plastic zone propagates as the compressibility of formation decreases, which is compatible with the effect of Poisson's ratio on the size of plastic zone.

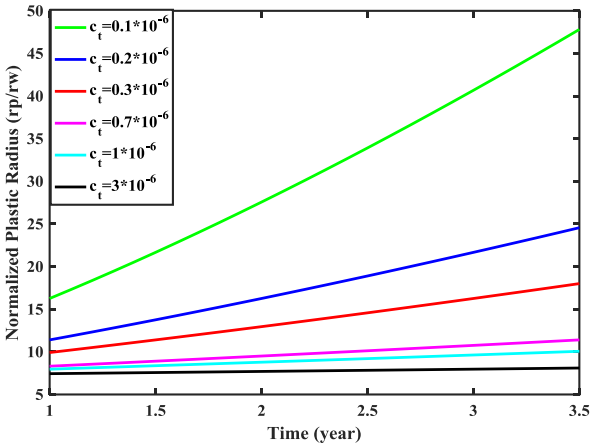

Fig. 11: Effect of rock compressibility on radius of plastic zone

The effect of Biot-Wilis coefficient on the radius of plastic zone is described in **Fig. 12**. As this figure shows, the radius of plastic zone progresively enlarges as the Biot-Willis coefficeint increases. This coefficient is a measure of contribution of pore pressure in total stresses and therefore the higher values of this parameter implies a higher pore pressure contribution (or lower effective stress). Moreover, the rate of growth of plastic zone increases with time.

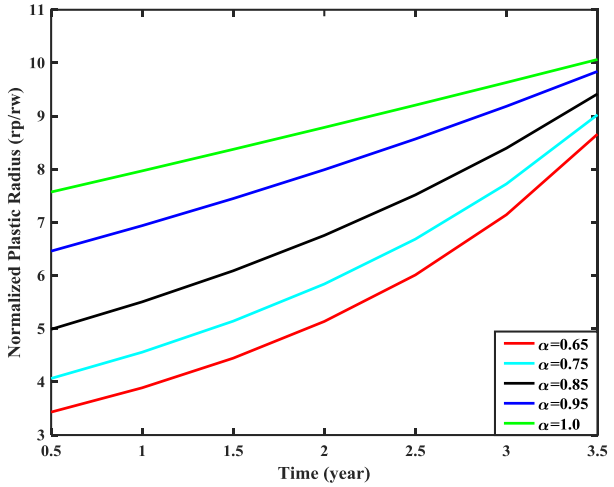

Fig. 12: Effect of Biot-Willis coefficient on radius of plastic zone

Petrophysical properties

The effect of porosity on the size of plastic region is given in **Fig. 13**. As this plot shows, the higher porosity, the smaller the size of plastic region. From equation (4), the diffusivity coefficient increases with porosity. This means that the pressure disturbance is transmitted faster and consequently lower pore pressure occurs in the formation and this implies higher resistance to failure (or smaller plastic radius).

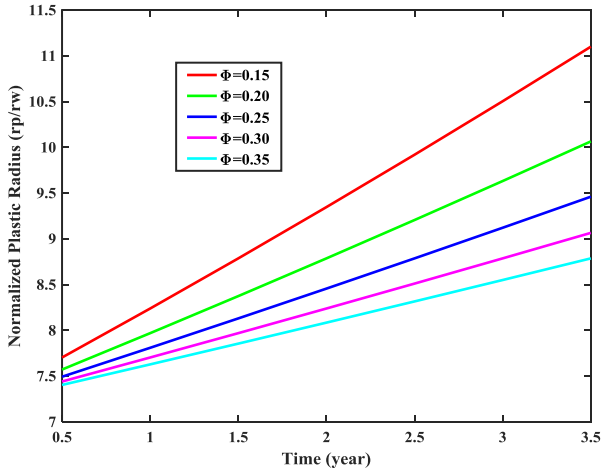

Fig. 13: Effect of porosity on radius of plastic zone

Fig. 14 indicates the effect of formation intrinsic permeability (single phase flow) on radius of plastic zone for a cohesive strength and friction angle of 440 psi and 15°, respectively. The size of plastic zone is larger for lower values of permeability. The reason for this is that in the higher permeability formations, the pore pressure dissipates faster than the low permeability formations. As a result, the lower permeability horizons are more prone to depletion-induced shear failure.

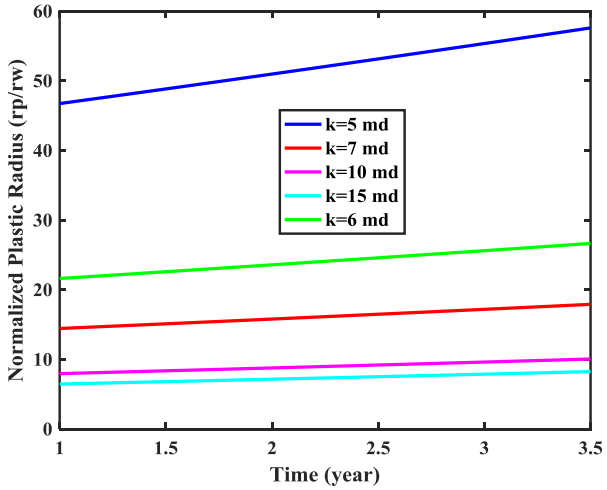

Fig. 14: Effect of permeability on radius of plastic zone

Fluid properties

Fig. 15 shows the plot of normalized plastic radius as a function of time and the production fluid viscosity for a cohesive strength and friction angle of 440 psi and 15°, respectively. The size of plastic zone is progressively larger for higher viscosities. This behavior is because of the effect of viscosity on the pore pressure distributions in the reservoir. The higher viscosity, the slower pressure transmission. This implies that the pore pressure dissipates slowly for higher viscosities and this means lower effective stress and more possibility for shear failure.

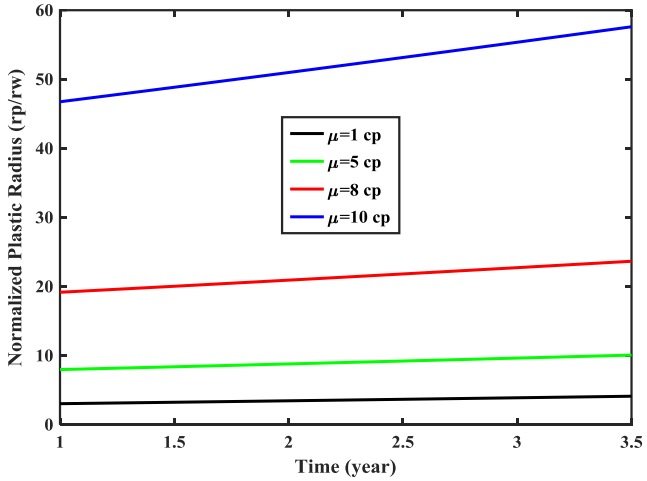

Fig. 15: Effect of fluid viscosity on radius of plastic zone

Operational factors

Fig. 16 is a plot of normalized plastic radius development for a cohesive strength and friction angle of 440 psi and 15°, respectively. The fluid viscosity used for this simulation is 1 cp. The plastic zone propagates as the wellbore pressure reduces with time. The radius of plastic region increases as flow rate increases from 380 bbl/d to 860 bbl/d. Moreover, the plot indicates that at higher flow rates the rate of growth of plastic zone is higher.

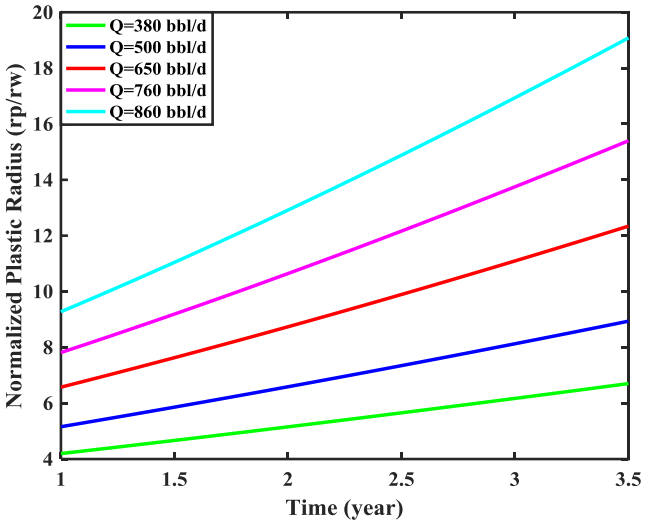

Fig. 14: Effect of flow rate on radius of plastic zone

Conclusion

Prediction of the effect of pressure drawdown on the stress distribution and the size of plastic region around the wellbore is critical for design of sanding control strategies as well as borehole integrity assurance in the partially depleted reservoirs. Since the flow regime is dominantly pseudo steady state in depleted reservoirs, the transient flow regimes cannot be utilized. In this study, a model was proposed to predict the stress state around the wellbore based on the theory of brittle elastoplasticity. According to the results, the stresses in the plastic region relieve compared to the elasticity-based solutions. In addition to this, the effect of various parameters on the radius of plastic zone was investigated. The results indicate that there are several controllable and uncontrollable factors, which affect the radius of plastic region. The uncontrollable parameters include rock and fluid properties as well as the initial in-situ stresses and pore pressure. The controllable parameters are wellbore pressure and the production flow rate. For the case of the constant production flow rate, the rate must be kept in such a way that the wellbore pressure remains higher than the critical flow rate. The model has the capability to obtain the critical flow rate to prevent excessive sanding during production.

Nomenclature

Symbol	Description
K	Bulk modulus of porous material
G	Shear modulus
ν	Poison's ratio
α	Biot-Willis coefficient
k	Permeability
ϕ	Porosity
σ_{ij}	Stress tensor components i,j: r,θ,z
ε_{ij}	Strain tensor components i,j: r,θ,z
p	Pore pressure
σ_h	Minimum horizontal in-situ stress
σ_v	Overburden in-situ stress
p_i	Initial reservoir pressure
δ_{ij}	Kronecker delta
u	Displacement in horizontal direction
r_w	Wellbore radius
r_e	Reservoir's outer boundary radius
h	Reservoir thickness

References

Aadnoy, B.S. (1991). Effect of reservoir depletion on borehole stability. Journal of petroleum science and engineering, 6, pp. 57-61.

Addis, M.A. (1997a). Reservoir depletion and its effect on wellbore stability evaluation. Int. J. Rock Mech. & Min. Sci, 34: 3-4.

Biot, M.A. (1941). General theory of three-dimensional consolidation. Journal of Applied Science, 12(2): pp.155-164.

Baldino, S., Rafieepour, S., Miska, S. Z. (2017), In-Situ Poisson's Ratio Determination Under Different Deformational Conditions, SPE 185112, SPE Oklahoma City Oil and Gas Symposium, Oklahoma City, USA.

Bradford, I.D.R., Cook, J.M. (1994). A semi-analytic elastoplastic model for wellbore stability with application to sanding. SPE 28070. 1994 Eurock SPE/ISRM Rock Mechanics in Petroleum Engineering Conference held in Delft, the Neatherlands, 29-31 August 1994.

Bradley, W.B. (1979a). Failure of inclined boreholes. J. Energy Resources Technology, 101, pp. 233-239.

Bradley, W.B. (1979a). Mathematical concept stress cloud can predict borehole stability . Oil and Gas Journal, 101, pp. 93-102.

Brown, E. T., Bray, J. W., Ladanyi, B., and Hoek, E. (1983). Ground response curves for rock tunnels J. Geotech. Engr. Div., 109(1),15–39.

Chen, S. L., Abousleiman, Y. N., Muraleetharan, K.K. (2012), Closed-form elastoplastic solution for the wellbore problem in strain hardening/softening rock formations. Intl. J. of Geomech. DOI: 10.1061/(ASCE)GM.1943-5622.0000157.

Chen, H., Teufel, L.W., Lee, R.L. (1995). Coupled fluid flow and geomechanics in reservoir study-I. Theory and governing equations. SPE 71087, SPE Rocky Mountain Petroleum Technology Conference, 21-23 may, Keystone, Colorado.

Chen, H., Teufel, L.W. (2001). Reservoir stress changes induced by production/injection. SPE 71087, SPE Rocky Mountain Petroleum Technology Conference, 21-23 may, Keystone, Colorado.

Dake, L.P. (1998). Fundamentals of reservoir engineering. Elsevier science, The Netherlands.

Hettema, M.H.H., Schutjens, P.M.T.M., Verboom,B.J.M., Gussinkio,H.J. (2000). Production-induced compaction of a sandstone reservoir: The strong influence of stress path. SPE Reservoir Eval. & Eng., 3(4), pp. 342-347.

Holt, R.M. (2004). Consequences of depletion-induced stress changes on reservoir compection and recovery. 6th North America Rock Mechanics Symposium held in houston, TX.

Jaeger, J.C., Cook, N.G.W., Zimmerman, R.W. (2007). Fundamental of rock mechanics (Fourth Edition ed.). Blackwell publishing.

McLellan, P.J., Wang, Y. (1994). Predicting the effcets of pore pressure penetration on the extent of wellbore instability: Application of a versatile poro-elastoplastic model. SPE 28053. 1994 Eurock

SPE/ISRM Rock Mechanics in Petroleum Engineering Conference held in Delft, the Neatherlands, 29-31 August 1994.

Morita, N., Whitfill, D.L., Nygaard, O., Bale, A. (1989). A quick method to determine subsidence, reservoir compaction and in-situ stress induced by reservoir depletion. Journal of Petroleum Technology, pp. 75-84.

Paslay, P.R., Cheatham JR., J.B. (1963). Rock stresses induced by flow of fluids into boreholes. SPE Journal, 3, pp. 85 – 94.

Papanastasiou, P., and Durban, D. (1997). Elastoplastic analysis of cylindrical cavity problems in geomaterials. Int. J. Numer. Anal. Methods Geomech., 21(2), 133–149.

Rafieepour, S., Jalayeri, H., Ghotbi, C., Pishvaie, M.R. (2015a). Simulation of wellbore stability with thermo-hydrochemo-mechanical coupling in troublesome formations:an example from Ahwaz oil field, SW Iran Arab Journal of Geoscience. 8, pp. 379–396.

Rafieepour, S., Ghotbi, C., Pishvaie, M.R. (2015b). The effects of various parameters on wellbore stability during drilling through Shale formations. Petroleum Science and Technology, 33, pp.1275–1285.

Rafieepour, S., Miska, S.Z., Zhang, J., Majidi, R.. "Poroelastoplastic modeling of reservoir in-situ stress change and deformation during depletion and injection". Revised at J. of Nat. Gas. Sci. and Eng., Elsevier, 2017.

Rafieepour, S., Miska, S.Z.Spatio-temporal stress path under different deformational conditions. Accepted at ASME 2017 36th International Conference on Ocean, Offshore and Arctic Engineering OMAE2017 June 25-30, Trondheim, Norway.

Rafieepour, S., Miska, S.Z. (2017). Geomechanical well testing: A new methodology for interpretation of pressure transient testing data for geomechanical applications. Accepted at SPE Annual Technical Conference (ATCE), San Antonio, TX.

Risnes, R., Bratli, R. K., Horsrud, P., 1982. Sand Stresses around a Wellbore. SPE Journal, 22(6), pp. 883-898.

Santarelli, F.J.,Tronvoll, J.T., Svennekjaer, M., Skeie, H., Henriksen, R., Bratli, R.K. (1998). Reservoir stress path: The depletion and the rebound. SPE/ISRM 47350 Eurock '98 held in Torenheim, Norway, 8-10 July.

Segall, P. (1985). Stress and subsidence resulting from subsurface fluid withdrawal in the epicentral region of the 1983 Coalinga Earthquake. Journal of Geophysical Research, 90(B8), pp.6801-6816.

Segall, P. (1989). Earthquakes triggered by fluid extraction. Geology, 17, pp. 942-946.

Seth, M.S., and Gray, K.E. 1967a. Transient Stresses and Displacement around a Wellbore Due to Fluid Flow in Transversely Isotropic, Porous Media: I. Infinite Reservoirs. SPE Journal, 8(1), pp. 63 – 78.

Seth, M.S., and Gray, K.E. 1967b. Transient Stresses and Displacement around a Wellbore Due to Fluid Flow in.Transversely Isotropic, Porous Media: II. Finite Reservoirs. SPE Journal, 8(1), pp. 79 – 86.

Shahri, M.P., Miska, S. (2013). Spatio-temporal stress path prediction using a fluid flow-geomechanical model. SPE Anual Technical Conference and Exhibition held in New Orlean, Louisiana, USA.

Wang, H. and Sharma, M.M. (2016). A fully 3-D, multi-phase, poro-elasto-plastic model for sand production. SPE-181566-MS, SPE Annual Technical Conference and Exhibition, 26-28 September, Dubai, UAE.

Wang, H. (2000). Theory of linear poroelasticity with applications to geomechanics and hydrogeology. Princeton University Press.

Wang Y., Dusseault, M.B. (1994). Stresses around a circular opening in an elastoplastic porous medium subjected to repeated hydraulic loading. Int. J. Rock Mech. Min. Sci. and Geomech. Abstr. 31 (6), pp. 597-616.